

# Tracing magnetism and pairing in FeTe-based systems

K. Palandage,<sup>1,\*</sup> K. Fang, G. W. Fernando,<sup>2,†</sup> and A. N. Kocharian<sup>3</sup>

<sup>1</sup>*Department of Physics, Trinity College, Hartford, CT 06106*

<sup>2</sup>*Department of Physics, University of Connecticut, Storrs, CT 06269*

<sup>3</sup>*Department of Physics and Astronomy, California State University, Los Angeles, CA 90032*

In order to examine the interplay between magnetism and superconductivity, we monitor the non-superconducting chalcogenide FeTe and follow its transitions under insertion of oxygen, doping with Se and vacancies of Fe using spin-polarized band structure methods (LSDA with GGA) starting from the collinear and bicollinear magnetic arrangements. We use a supercell of  $\text{Fe}_8\text{Te}_8$  as our starting point so that it can capture local changes in magnetic moments. The calculated values of magnetic moments agree well with available experimental data while oxygen insertions lead to significant changes in the bicollinear or collinear magnetic moments. The total energies of these systems indicate that the collinear-derived structure is the more favorable one prior to a possible superconducting transition. Using a 8-site Betts-cluster-based lattice and the Hubbard model, we show why this structure favors electron or hole pairing and provides clues to a common understanding of charge and spin pairing in the cuprates, pnictides and chalcogenides.

PACS numbers: 65.80.+n, 73.22.-f, 71.27.+a, 71.30.+h

High temperature superconductors discovered in the 1980s consisted of copper-oxide-based, layered materials. In such cuprates, it is believed that doping, away from half filling, of a Mott-insulator leads to superconductivity although there is still no general agreement on a specific mechanism. Recently discovered superconductivity in Fe-based compounds, which are either pnictides or chalcogenides [1, 2], has opened up an extremely rich and active area of basic research. Although the transition temperatures of the Fe-chalcogenide superconductors are among the lowest of the recently discovered compounds, they possess rather simple layered structures and fascinating antiferromagnetic or spin density wave (SDW) states. Superconductivity in the Fe-chalcogenides, having the so-called (11) structure, was first reported in 2008 (Refs. [2, 3]) in  $\text{Fe}_{1+\delta}\text{Se}$  and  $\text{Fe}(\text{Se}_{1-x}\text{Te}_x)_{0.82}$ . This discovery led to a substantial increase in research efforts focused on simple, layered Fe compounds, containing chalcogenides such as S, Se, and Te. FeTe, which is a metallic antiferromagnet, has a tetragonal structure and has shown properties uniquely different from some of the other pnictides and chalcogenides. For example,  $\text{Fe}_{1+\delta}\text{Te}$  is not superconducting; instead, it shows magnetic and structural transitions at 65 K [4]. In addition, it is said to have the so-called “double stripe” antiferromagnetic order instead of the “single stripe” with ordering vector  $(0.5, 0.5)$  [5]. Nevertheless, FeTe doped with Se was found to be superconducting (Refs. [1, 6]). Oxygen insertions in FeTe (films) have also given rise to superconductivity (Refs. [7, 8]). There are claims that the Fe-chalcogenides do not exhibit the same nesting feature found in the pnictides and that they possess a different local SDW magnetic order which survives even in the highest  $T_c$  samples [9].

The present work is focused on understanding such changes while attempting to find common behavior, es-

pecially en route to superconductivity, in these chalcogenide (and possibly pnictide and cuprate) systems. We note that there have been numerous band structure calculations carried out recently on related systems focusing on nesting features of the relevant Fermi surface, susceptibilities among other things (see Ref. [10] and references therein); however, to our knowledge, these studies have not focused on systematic changes in the resulting moments and/or total energy as functions of various modulations en route to superconductivity.

## Band structure

Our band structure calculations are based on the (spin-polarized) density functional theory (DFT) [11, 12], combined with the generalized gradient approximation (GGA) [13], as implemented in the VASP package [14–16]. The interaction between the electrons and atomic cores is described by projector augmented wave (PAW) pseudopotentials. The wave functions are expanded using plane waves with a cut of energy of 400 eV. Brillouin Zone integrations are carried out with a  $4 \times 4 \times 4$  Monkhorst-Pack [17] grid of k-points while a denser  $8 \times 8 \times 8$  k-point mesh was used for the density of states (DOS) calculations. The lowest energy structure was determined using Broyden-Fletcher-Goldfarb-Shanno (BFGS) [18] based algorithms. For the results reported in this work, all the atoms are allowed to relax based on Hellman-Feynman forces and optimization is carried out until typical forces on the atoms are around 0.01 eV/Å or less.

FeTe has a tetragonal structure with space group  $P4/nmm$ , where a square lattice of Fe is tetrahedrally coordinated with Te ions. Experimental lattice parameters of the pure FeTe are  $a = b = 3.8248 \text{ Å}$  and  $c = 6.2910 \text{ Å}$ ;

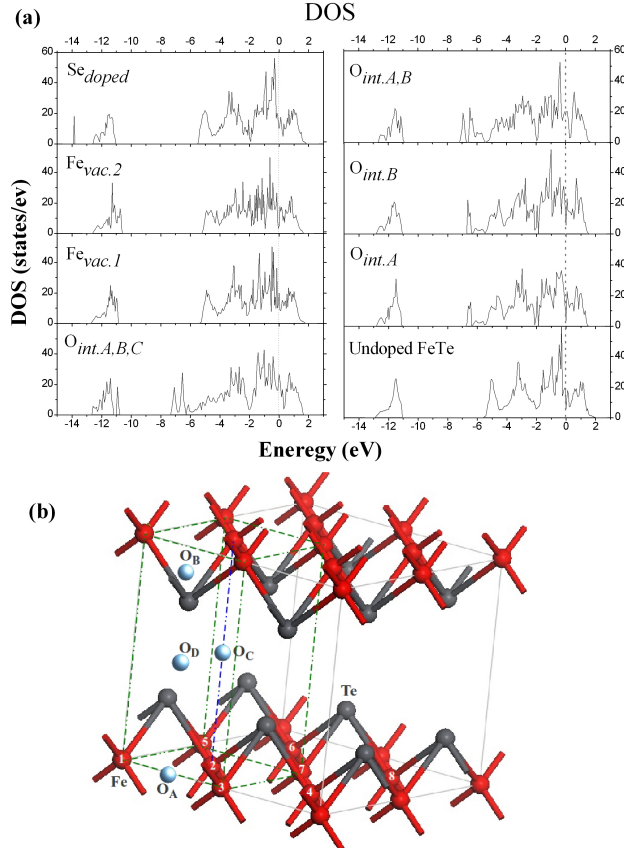


FIG. 1: Projected FeTe density of states due to various modulations and the supercell studied here; Fe atoms are located on the plane shown and possible oxygen interstitial sites are identified as A, B, C and D; Te atoms are gray spheres in between the planes of Fe.

these were used as the starting lattice parameters for the  $2 \times 2 \times 1$  supercell. This 16-atom tetragonal supercell, consists of 8 Fe and 8 Te atoms (see Fig. 1(b)) with Fe atoms located in a plane with Te atoms sitting above (and below) the plane. The reason for choosing a large supercell is to examine possible nontrivial SDW-type behavior; i.e., to allow moments to (vary and) align among themselves as necessitated by the variational principle in total energy. A smaller cell will not have such freedom. Following the (non-spin-polarized) work of Ref. [7], the interstitial sites for oxygen insertion (A, B, C, D in Fig. 1(b)) were selected by comparing the total energies of several possible interstitial sites containing oxygen in the unit cell. Although our spin-polarized work shows some differences (related to sites C and D) with the above unpolarized work, sites A and B (for oxygen interstitials) appear to be the most energetically favorable, as deter-

mined there.

The other modulations studied in this work are; (a) Fe interstitials, (b) Fe vacancies and (c) Se dopants. It is experimentally known that, except in case (a), these changes to pure FeTe, carried out with sufficient care, are likely to induce superconductivity. We note that without the GGA, the calculated moments turn out to be rather small and (quantitative) conclusions drawn from pure LDA (or LSDA) work alone may be questionable.

### Magnetic Moments

The magnetic moments in pure FeTe and its various modulations were calculated starting from two different (AFM) magnetic structures, collinear and bicollinear (see Fig. 5). Note that in the collinear structure,  $\vec{k} = (0.5, 0.5)$  (with respect to a 2-Fe unit cell) antiferromagnetic order is present while the bicollinear structure has  $(0.5, 0.0)$  order. The pure compound FeTe, in both magnetic structures, carry Fe moments which are around  $2.0 \mu_B$ , in agreement with recent experiments. This fact alone points to the relevance and importance of multi-orbital effects at the Fermi surface since otherwise the moments cannot be this high. Our density of states plots (Fig. 1(a)) identify these as originating from d-orbitals, which is not a surprise. These moments are found to be severely affected by the insertion of two oxygen atoms into interstitial sites A and B (see Table I and II); Four of the eight Fe atoms show moments that are around  $1.2 \mu_B$  or less while the total charge in each atom undergoes minimal (less than one percent) changes. In density functional calculations based on various approximations such as the LDA or GGA, such changes are not unusual. Hence, one cannot make specific statements about changes in the valence (such as  $\text{Fe}^{2+} \rightarrow \text{Fe}^{3+}$ ) using these results alone. However, when the total valence charges of Te and O are compared (at the same radii), there is a clear difference. Oxygen has more charge while being more electronegative and hence, its insertion is likely to create holes in the Fe atoms.

Insertion of Fe into A and B interstitial sites of FeTe does not appear to change the moments as drastically. In fact, while the moments of the Fe atoms in FeTe are almost unchanged, showing long-ranged antiferromagnetic order, the inserted Fe atom carries a moment of about  $2.46 \mu_B$ , close to the value reported by some experiments [19]. The variationally determined total energies of these two, collinear and bicollinear, structures show a trend that supports experimental findings for FeTe and Se-doped FeTe. With the pure system exhibiting collinear (static) antiferromagnetic (AFM) ground state,

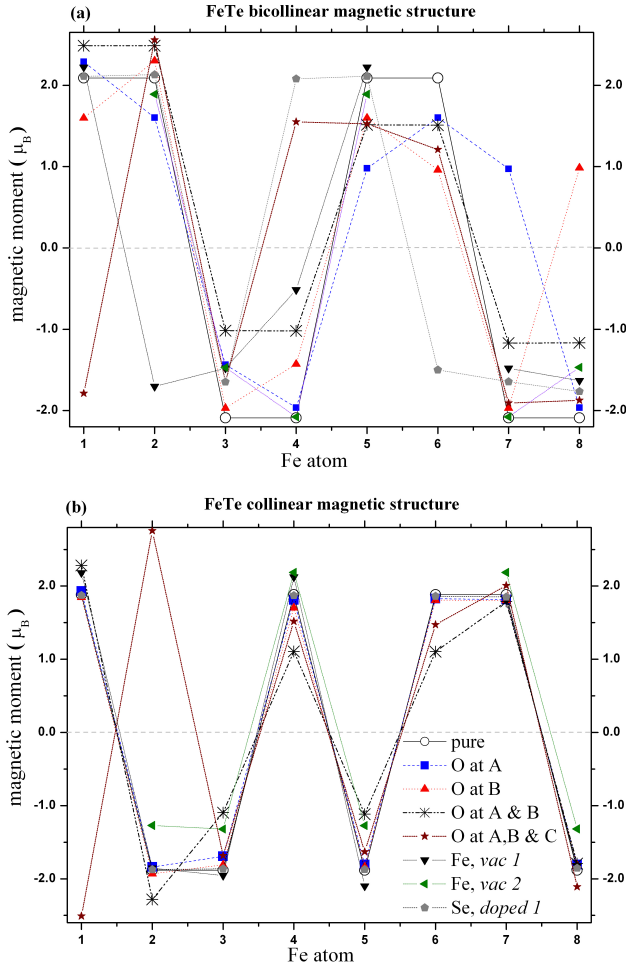


FIG. 2: Damped antiferromagnetic or SDW arrangements as calculated for bicollinear (top) and collinear (bottom) Fe arrangements. Atom labels are as in Fig. 1.

we have examined the iron or oxygen inserted systems (Fe or oxygen at A and B sites, as shown in Fig. 1 and Tables I and II in addition to other modulations. Interestingly, the ground state magnetic structure of FeTe-Fe appears to depend on the extra Fe content. As reported in Ref. [6], in  $\text{Fe}_{1+\delta}\text{Te}$ , the favored magnetic structure is the bicollinear one as our calculations indicate for  $\delta=0.125$ . For  $\delta = 0$ , the situation is reversed and the difference in total energy between the two phases with  $\delta = 0$  and  $\delta = 0.125$  is less than 0.2 eV (per supercell). The two magnetic states appear to be competing to be the ground state, with total energies that are quite close to one another.

However, with oxygen insertion, this situation changes noticeably; with oxygen occupying either site A or site

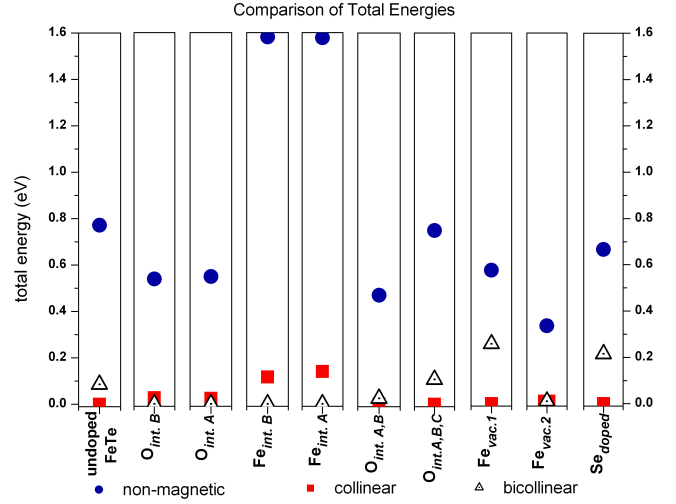


FIG. 3: Comparisons of total energies of Fe-Te magnetic structures with various modulations. Note that the collinear structure is the more favorable one prior to going into a possible superconducting state.

B, the bicollinear arrangement becomes more stable with some rearrangements in the (magnitude and direction of) magnetic moments. However, with oxygen occupying both A and B sites, the collinear structure (with reduced/different moments) becomes the more stable one. We emphasize that this is an experimentally observed trend (Ref. [6]). There is clearly no true antiferromagnetism here; instead, we see some Fe moments reduced by as much as 30-50% while others show smaller changes. We will label such magnetic states as damped SDW states. Our unit cell contains 8 Fe atoms and hence it is able to show the damping/oscillations better than what would be seen in a small (say  $\text{Fe}_2\text{Te}_2$ ) cell; a larger supercell with more Fe atoms is likely to show the damping or oscillatory effects even better. In general, experiments show that static magnetism hinders superconductivity while spin fluctuations, which increase dramatically as the superconducting transition temperature  $T_c$  is approached, help or act as a precursor to it in the cuprates, pnictides and chalcogenides. Another point to note is the reduction in some Fe-site moments in the  $\text{Fe}_{8-\alpha}\text{Te}_8$  calculation with two vacancies in the collinear structure; however, in every case some notable local magnetic order is still present.

We believe that, although the true, static antiferromagnetism vanishes with the above modulations, local magnetic order plays a crucial role at least as a precursor to superconductivity. There is new evidence for such

| Collinear                 |             |            |      |     |      |     |     |      |
|---------------------------|-------------|------------|------|-----|------|-----|-----|------|
| Fe Atom #                 | 1           | 2          | 3    | 4   | 5    | 6   | 7   | 8    |
| Initial Moment            | ↑           | ↓          | ↓    | ↑   | ↓    | ↑   | ↑   | ↓    |
| Pure                      | 1.9         | -1.9       | -1.9 | 1.9 | -1.9 | 1.9 | 1.9 | -1.9 |
| $O_{intA}$                | 1.9         | -1.8       | -1.7 | 1.8 | -1.8 | 1.8 | 1.8 | -1.8 |
| $O_{intB}$                | 1.8         | -1.9       | -1.8 | 1.7 | -1.8 | 1.8 | 1.8 | -1.8 |
| $O_{intA,B}$              | 2.3         | -2.3       | -1.1 | 1.1 | -1.1 | 1.1 | 1.8 | -1.8 |
| $O_{intA,B,C}$            | <b>-2.5</b> | <b>2.8</b> | -1.7 | 1.5 | -1.6 | 1.5 | 2.0 | -2.1 |
| $Fe_{vac.6}$              | 2.2         | -1.9       | -2.0 | 2.1 | -2.1 | -   | 1.8 | -1.8 |
| $Fe_{vac.1,6}$            | -           | -1.3       | -1.3 | 2.2 | -1.3 | -   | 2.2 | -1.3 |
| $Se_{sub.doped}(Te_{15})$ | 1.9         | -1.9       | -1.9 | 1.9 | -1.9 | 1.9 | 1.9 | -1.9 |

TABLE I: Calculated collinear magnetic moments of Fe atoms for different configurations. Atom labels are as in Fig. 1 and initial magnetic moment direction changes are highlighted in bold face.

| Bicollinear               |             |             |      |            |     |      |            |            |
|---------------------------|-------------|-------------|------|------------|-----|------|------------|------------|
| Fe Atom #                 | 1           | 2           | 3    | 4          | 5   | 6    | 7          | 8          |
| Initial Moment            | ↑           | ↑           | ↓    | ↓          | ↑   | ↑    | ↓          | ↓          |
| Pure                      | 2.1         | 2.1         | -2.1 | -2.1       | 2.1 | 2.1  | -2.1       | -2.1       |
| $O_{intA}$                | 2.3         | 1.6         | -1.4 | -2.0       | 1.0 | 1.6  | <b>1.0</b> | -2.0       |
| $O_{intB}$                | 1.6         | 2.3         | -2.0 | -1.4       | 1.6 | 1.0  | -2.0       | <b>1.0</b> |
| $O_{intA,B}$              | 2.5         | 2.5         | -1.0 | -1.0       | 1.5 | 1.5  | -1.2       | -1.2       |
| $O_{intA,B,C}$            | <b>-1.8</b> | 2.6         | -1.6 | <b>1.6</b> | 1.5 | 1.2  | -1.9       | -1.9       |
| $Fe_{vac.6}$              | 2.2         | <b>-1.7</b> | -1.5 | -0.5       | 2.2 | -    | -1.5       | -1.6       |
| $Fe_{vac.1,6}$            | -           | 1.9         | -1.5 | -2.1       | 1.9 | -    | -2.1       | -1.5       |
| $Se_{sub.doped}(Te_{15})$ | 2.1         | 2.1         | -1.6 | <b>2.1</b> | 2.1 | -1.5 | -1.6       | -1.8       |

TABLE II: Calculated bicollinear magnetic moments of Fe atoms for different configurations. Atom labels are as in Fig. 1.

behavior seen even in the cuprates. Recent RIXS (resonant inelastic X-ray scattering) experiments on the 123 cuprate have revealed an intense peak around 1.7 eV energy loss that is due to an optically forbidden  $d-d$  transitions of unpaired holes from  $Cu2^+$  to other d-orbitals (Ref. [20]). The significance of this work is that in overdoped, underdoped and superconducting samples, magnetic excitations are seen around the same energy region.

### Total energies

A comparison of variationally evaluated total energies is one of the most useful and reliable outputs of a DFT-based calculation. Various modulation-induced structures were selected since, experimentally, these were identified as necessary precursors for FeTe-derived super-

conductivity. Total energies shown in Fig. 3, for all the modulated structures show a very clear trend; i.e., the collinear-derived magnetic structure becomes the more favorable one prior to possible superconducting transitions.

Here is a brief summary for the various structures: (a) Pure  $Fe_8Te_8$ : Collinear structure is more stable with Fe magnetic moments about  $2\mu_B$  per atom. (b)  $Fe_9Te_8$ : Bicollinear is more stable with the extra Fe atom carrying a moment of about  $2.5\mu_B$ . (c) Oxygen interstitial: Inserting one oxygen atom either at the interstitial site A or B brings the total energies of the two magnetic structures close to one another and two inserted oxygens make it even closer. With three inserted oxygens, the collinear structure clearly becomes the more favorable. (d) Introduction of a single vacancy into the supercell induces a clear separation of the total energies with collinear one being more stable; nevertheless, a second vacancy brings their energies closer together. (e) Se doping makes the collinear structure more stable.

While a one particle mean-field theory alone is unlikely to explain pairing related phenomena in moderately correlated systems, the trends seen with oxygen insertions, Fe vacancies and Se doping appear to confirm several experimental findings, such as short-range magnetic order [21]. The true, static AFM state, with large Fe moments, is lost due to oxygen insertions and other doping while some remnants of this lost state can be gleaned from the band calculations. However, without further assumptions and work, these results alone are unable to demonstrate a pairing scenario as to where the holes are created and their role due to these modulations. This is not surprising since it is well known that the local approximations to exchange-correlation and mean-field effects usually wipe them out. In addition, Fermi surface topology-based nesting mechanisms have become popular and have been used to obtain various pairing mechanisms. However, in view of the loss of long range antiferromagnetic order and the onset of short range incommensurate order observed experimentally (Ref. [21]) and suggested by our supercell calculations, we present a different pairing scenario, based on a spatially local mechanism, in the following section.

### Charge and spin Pairing

Here we introduce a many-body, Hubbard Hamiltonian where explicit fluctuations of paired holes can be systematically studied in a grand canonical ensemble [22, 23]. Such calculations on a 8-site Betts cluster-based lattice (see Fig. 4) show that there are instabilities/fluctuations

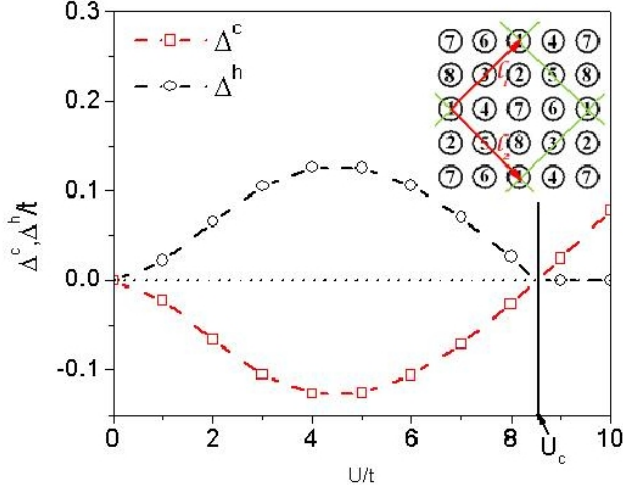


FIG. 4: Negative charge gap and positive spin gap in the 8-site Betts-cluster-based lattice. The 8-site Betts cell, which is periodically repeated with edge vectors (2,2) and (2,-2), is also shown here.

in charge and spin degrees of freedom under “suitable” conditions. These fluctuations exist between a background AFM/SDW state and a two hole- or electron-doped state in a phase region identified as having a negative charge gap favoring charge and spin pairing (at a critical value of doping). Although our recent work [24] refers to a single orbital model, we infer that it can be extended to two or multi-orbitals and still retain the negative charge gap, as long as hopping strength among similar orbitals is greater than that for different ones.

Depending on the value of the electron-electron Coulomb repulsion  $U$ , there are certain regions in a 3-dimensional  $T(\text{temperature})$ - $\mu(\text{chemical potential})$ - $U$  phase space where quantum critical points (QCPs) exist and drive these fluctuations. For the 8-site Betts cluster-based lattice, with periodic boundary conditions, such a QCP has been found at  $U = U_c = 8.54$  (in units of  $t$ , the hopping parameter in the Hubbard model), so that a charge instability exists in the region  $0 < U < U_c$  at suitable (doping)  $\mu = \mu_c$  and  $T$ . This charge instability leads to fluctuations between a SDW/AFM state and a state with extra holes of paired (and unlike) spins at low temperature. Note that even for very small  $U$  (i.e., weakly correlated systems), a negative charge gap and a coherent (positive) spin gap can exist. Our grand conical ensemble-based studies show that these paired spins are stabilized by the (positive) spin gap up to a temperature

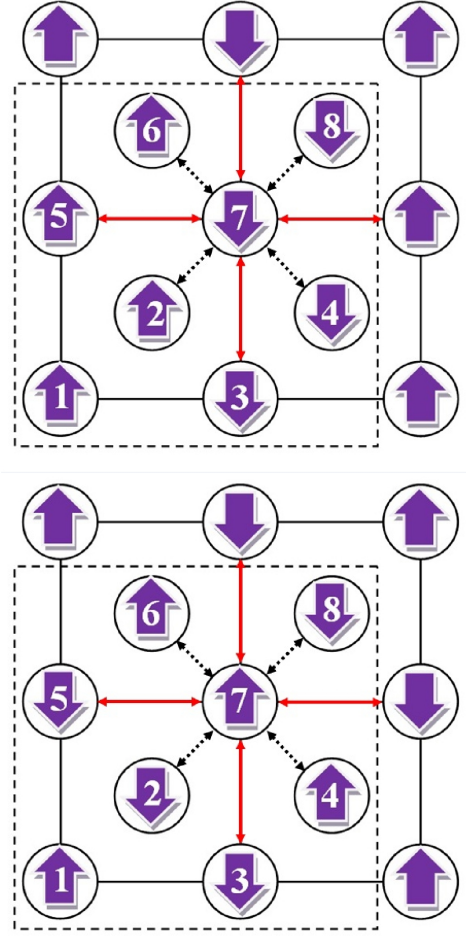


FIG. 5: Bicollinear (Top) and collinear (bottom) magnetic structures in the plane containing Fe atoms. Arrows identify nearest and next nearest neighbors of the seventh atom (as marked) in the plane.

$T_s$ . Clearly, with extra holes, it is easier for the charge carriers to move between sites, as seen in the oxygen-doped case.

An important point here is that such a scenario favors a background of collinear-derived states discussed in the previous sections, rather than the bicollinear one. This is simply due to the differences in the neighboring spins which begin to appear at the next nearest neighbor (nnn) level of the two structures (see Fig. 5). For an electron (or a hole) to hop through the lattice and form a pair, existence of (as many) unlike-spins as next nearest neighbors would be an asset (since like-spin neighbors would prevent hopping to that orbital) provided that  $U$  values are relatively small. This is what is seen in the collinear structure with 4 unlike-nnn-spins, compared to

2 unlike-*nnn*-spins in the bicollinear structure (while at the nearest neighbor level, there is no difference). Our calculated charge gap for the 8-site Betts-cluster-based lattice shows that the next nearest neighbor hopping, under certain conditions, can play a crucial, helpful role in the charge and spin pairing instability [24].

### Summary

Our band calculations, which are consistent with several experimental results, are used to identify states that act as precursors to superconductivity. In every case considered for the Fe-chalcogenide under consideration, a collinear-derived, damped SDW is predicted. A theory based on the Hubbard model, with a weak onsite Coulomb repulsion, is able to explain possible charge and spin fluctuations starting from these precursors. We believe that this work lays the ground work for a common understanding of superconductivity in the chalcogenides, pnictides and cuprates.

### Acknowledgments

We thank Profs. J. I. Budnick and B. O. Wells for useful discussions. The authors also acknowledge the computing facilities provided by the Center for Functional Nanomaterials, Brookhaven National Laboratory, which is supported by the U.S. Department of Energy, Office of Basic Energy Sciences, under Contract No. DE-AC02-98CH10886.

<sup>†</sup> Electronic address: fernando@phys.uconn.edu

- [1] Y. Kamihara, T. Watanabe, M. Hirano, and H. Hosono, *J. Am. Chem. Soc.*, **130**:3296, (2008).
- [2] Fong-Chi Shu et al., *Proc. Natl. Acad. sci. USA*, **105**:14262, (2008).
- [3] M. H. Fang et al., *Phys. Rev. B* **78**, 224503 (2008).
- [4] N. Katayama et al., *J. Phys. Soc. Jpn.*, **79**, 113702 (2010).
- [5] S. Li et al., *Phys. Rev. B* **79**, 054503 (2009); F. Ma et al., *Phys. Rev. Lett.*, **102**, 177003 (2009).
- [6] Z. Xu et al. *Phys. Rev. B* **82**, 104525 (2010).
- [7] Yufeng Nie et al., *Journal of Physics and Chemistry of Solids*, **72**, 426 (2011); Y. Nie et al., arXiv 0912.4539v1 (2009)
- [8] W. Si et al., *Phys. Rev. B* **81**, 092506 (2010).
- [9] Wei Bao et al., *Phys. Rev. Lett.*, **102**, 247001 (2009).
- [10] C-Y. Moon and H. J. Choi, *Phys. Rev. Lett.*, **104**, 057003 (2010).
- [11] P. Hohenberg, W. Kohn, *Phys. Rev.* **136**, (1964) B864.
- [12] W. Kohn, L. J. Sham, *Phys. Rev.* **140**, (1965) A1133.
- [13] J. P. Perdew et al., *Phys. Rev. Lett.* **76**, 3865 (1996).
- [14] G. Kresse, J. Furthmuller, *Phys. Rev. B* **54**, 11169, (1996).
- [15] G. Kresse, J. Furthmuller, *Comput. mater. Sci.* **6**, 15 (1996).
- [16] M. Shishkin, G. Kresse, *Phys. Rev. B* **74**, 035101 (2006).
- [17] H. J. Monkhorst, J. D. Pack, *Phys. Rev. B* **13**, 5188 (1976).
- [18] D. Vanderbilt, *Phys. Rev. B* **41**, 7982 (1990).
- [19] Martinelli et al. *Phys. Rev. B* **81**, 094115 (2010).
- [20] M. Le Tacon et al., *Nature Physics*, **7**, 725 (2011).
- [21] Jinsheng Wen et al., *Phys. Rev. B* **80**, 104506 (2009).
- [22] G. W. Fernando, K. Palandage, A. N. Kocharian, and J. W. Davenport, *Phys. Rev. B* **80**, 014525 (2009).
- [23] A. N. Kocharian, G. W. Fernando, K. Palandage, and J. W. Davenport, *Phys. Lett. A* **373**, 1074 (2009).
- [24] Kun Fang, G. W. Fernando and A. N. Kocharian (submitted to *Phys. Lett. A*).

---

\* Electronic address: kalum.palandage@trincoll.edu